Supporting Information

NIR Emission and Acid-Induced Intramolecular Electron Transfer Derived from a SOMO-HOMO Converted Non-Aufbau Electronic Structure

Akira Tanushi,[a] Shun Kimura,[a] Tetsuro Kusamoto,[a]* Moe Tominaga,[b] Yasutaka Kitagawa,[b] Masayoshi Nakano,[b,c] and Hiroshi Nishihara[a]*

[a]*Department of Chemistry, School of Science, The University of Tokyo, 7-3-1, Hongo, Bunkyo-Ku, Tokyo 113-0033, Japan*
[b]*Division of Chemical Engineering, Department of Materials Engineering Science, Graduate School of Engineering Science, Osaka University, Toyonaka, Osaka 560-8531, Japan*
[c]*Institute for Molecular Science, 38 Nishigo-Naka, Myodaiji, Okazaki 444-8585, Japan*

Contact author information
Tetsuro Kusamoto, Email: kusamoto@chem.s.u-tokyo.ac.jp.
Hiroshi Nishihara, Email: nisihara@chem.s.u-tokyo.ac.jp.

Table of Contents

Materials and methods

Materials

Water was purified using AUTOPURE WD500 (Yamato Scientific Co., Ltd.). Acetonitrile (MeCN), dichloromethane (CH_2Cl_2), diethyl ether (Et_2O), hexane, tetrahydrofuran (THF) and toluene used for synthesis were purified through organic solvent purifier (Nikko Hansen Co., Ltd.).

Equipments

NMR spectra were recorded with a Bruker US500 spectrometer at room temperature. Chemical shifts in ppm were referenced to tetramethylsilane (0.00 ppm) as an internal standard. MALDI-TOF mass spectra were recorded with a Shimazu KRATOS AXIMA-CFR TOF-MS spectrometer. UV-vis-NIR absorption spectra were recorded with a JASCO V570 spectrophotometer. Steady-state emission spectra were measured with HORIBA Fluorolog-3 spectrometer. ESR spectra were recorded with a JEOL JES-FA200 spectrometer. Observed *g*-values were calibrated with Mn^{2+}/MgO marker. Emission lifetime was recorded using a Hamamatsu Photonics Quantaurus-τ (C11367-22) with a picosecond light pulser (M12488-29).

Cyclic voltammetry was carried out under a N_2 atmosphere with a GC working electrode, a platinum wire counter electrode and an Ag^+/Ag reference electrode (10 mM $AgClO_4$ and 0.1 mM $^n Bu_4NClO_4$ in MeCN solution) with an ALS-650DT voltammetric analyzer. The platinum working electrode was polished with Al_2O_3 fine particles and washed with water and acetone with ultrasonication. The counter electrode was heated with oxygen flame to remove organic compounds on the surface and washed with acetone. The reference electrode was washed with acetone. The potential of the voltammograms is shown relative to the Fc^+/Fc redox couple.

DFT calculation

DFT calculations were carried out using Gaussian 09 program package.[1] The three-parameterized Becke-Lee-Yang-Parr (B3LYP) hybrid exchange-correlation functional[2-4] and long-range-corrected version of B3LYP using the Coulomb-attenuating method (CAM-B3LYP)[5] were employed with 6-31G* basis set.[6,7] The open-shell electronic structures were approximated by spin-unrestricted method. All molecular structures were optimized with those level of theories in the gas phase, and were confirmed by calculating the molecular vibrational frequencies, in which no imaginary frequencies were observed in any of the compounds. We also optimized the structure of TPA-R$^\bullet$ under a solvent (cyclohexane) condition with a polarizable continuum model (PCM) using the integral equation formalism variant (IEFPCM).[8] On the basis of this optimized structure, TD-DFT method was applied to calculate the excited states relevant to the absorption spectra in cyclohexane. B3LYP and CAM-B3LYP functional sets were used for the TD-DFT calculations with 6-31+G* basis set.

Estimation of emission quantum yield

Absolute emission quantum yield of TPA-R$^{\cdot}$ was measured using a Hamamatsu Photonics Quantaurus-QY Plus (C13534-02) with a high power Xe lamp unit and a NIR photoluminescence measurement unit. The quantum yields were 0.0010 and 0.0007 upon excitation at λ = 475 and 650 nm, respectively. The emission quanstum yield was also estimated based on the relative method using Indocyanine green as a standard. Indocyanine green is reported to display photoluminescence maximum wavelength at λ = 813 nm with the emission quantum yield of 0.106 upon excitation at λ = 694.3 nm.[9] The emission quantum yield of TPA-R$^{\cdot}$ calculated according to the literature procedure[10] was 0.0004 upon excitation at λ = 700 nm.

Synthesis and characterization

Synthesis of 2,3,5,6-tetrachlorotoluene

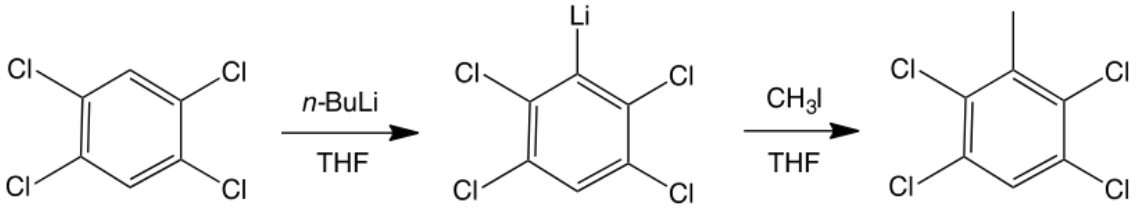

Under a N_2 atmosphere, to a mixture of tetrachlorobenzene 10.50 g (48.6 mmol) in anhydrous THF (200 mL) was added ^{n}BuLi (30 mL, 48.9 mmol) in 1.63 M hexane solution was added dropwise at –60°C ($CHCl_3$-CH_3CN-dry ice bath) (tetrachlorobenzene was not completely dissolved at –60°C). The mixture was stirred for an hour and the resulting pink solution was cooled to –78°C (acetone/dry ice bath). To the solution was added iodomethane 3 mL (48.2 mmol) in THF (30 mL) rapidly (not dropwise). Cooling was stopped, and the mixture was warmed to room temperature. The mixture was quenched with a water solution of $NaHCO_3$ and extracted with ether. The organic layer was separated and the aqueous layer was extracted with ether (100 mL×2). The extracts were combined with the organic phase, dried with $MgSO_4$. Evaporation of the solvent left a pale-yellow solid (10.44 g, 93 %). This crude product included little tetrachlorobenzene as impurity but was used in the next step without further purification. **^{1}H NMR** ($CDCl_3$, 500 MHz): 2.53 (s, 3H), 7.41 (s, 1H). **GC-MS**: *m/z* = 230 ($[C_7H_4Cl_4]^+$).

Synthesis of (3,5-dichloro-4-pyridyl)(2,3,5,6-tetrachloro-4-toluenyl)methanol

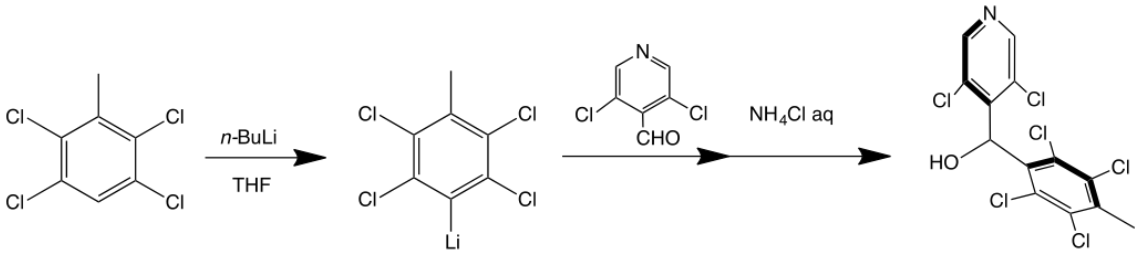

Under a N_2 atmosphere, to a solution of 2,3,5,6-tetrachlorotoluene (2.512 g, 10.9 mmol) in anhydrous THF (30 ml) was added dropwise a 1.60 M solution of ^{n}BuLi in hexane (8.8 mL, 10.6 mmol) at –78°C (acetone/dry ice bath). The brown mixture was stirred for 15 min at –78 °C, and was added 3,5-dichloro-4-pyridinecarboxaldehyde[11] (2.070 g, 11.8 mmol) in THF (20 mL). The resulting mixture was stirred for 2 h at –78°C, and was warmed up to room temperature. After addition of saturated aqueous NH_4Cl, the mixture was extracted with Ether. The organic layer was separated and the water layer was washed with ether (50 mL×2). The organic phase was collected, dried (Na_2SO_4) and filtered. Evaporation of the solvent gave yellow solid. The solid was washed with CH_2Cl_2 (30 mL) and became white solid (1.834 g, 43 %). This product was used in the next step without further purification. **^{1}H NMR ($CDCl_3$, 500 MHz)**: 2.62 (s, 3H), 3.41 (d, 1H, *J*=11 Hz), 6.85 (d, 1H, *J*=11 Hz), 8.44 (s, 2H). **GC-MS**: *m/z* = 405 ($[C_{13}H_7Cl_6NO]^+$).

Synthesis of (3,5-dichloro-4-pyridyl)(2,3,5,6-tetrachlorotoluenyl)(2,4,6-trichlorophenyl) methane (1)

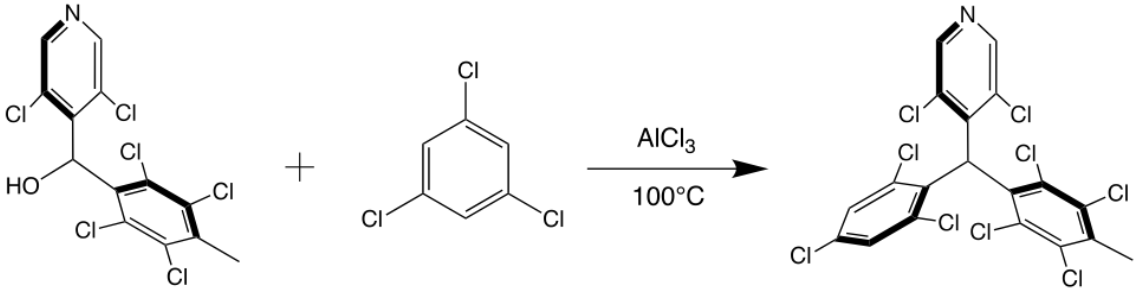

1

Under a N_2 atmosphere, a mixture of (3,5-dichloro-4-pyridyl)(2,3,5,6-tetrachloro-4-toluenyl)methanol (1.43 g, 3.5 mmol) and 1,3,5-trichlorobenzene (3.24 g, 17.5 mmol) and aluminum chloride (1.10 mg, 8.8 mmol) was heated to 100°C. The suspension (melting point of 1,3,5-trichlorobenzene is 63°C) was stirred for 20 h. The resulting dark-brown mixture was cooled to room temperature, dissolved in CH_2Cl_2 and added to ice water. The mixture was neutralized by aqueous $NaHCO_3$ and the organic layer was separated. The water layer was extracted with CH_2Cl_2 (3 times). The organic layers were combined, dried (Na_2SO_4), and evaporated. The crude product was purified by silica gel column chromatography (eluent: CH_2Cl_2/hexane = 1/1). Drying in vacuo gave white solid of (3,5-dichloro-4-pyridyl)(2,3,5,6-tetrachlorotoluenyl)(2,4,6-trichlorophenyl)methane (846 mg, 42%). This product was used in the next step without further purification. **^{1}H NMR ($CDCl_3$, 500 MHz)**: 2.62 (d, 3H, *J*=2.0 Hz), 6.80 (s, 1H), 7.25 (m, 1H), 7.37 (m, 1H), 8.36 (d, 1H, *J*=6.5 Hz), 8.47 (d, 1H, *J*=10 Hz). **GC-MS**: *m/z* = 569 ($[C_{19}H_8Cl_9N]^+$).

Synthesis of (3,5-dichloro-4-pyridyl)(4-bromomethyl-2,3,5,6-tetrachlorophenyl) (2,4,6-trichlorophenyl)methane (2)

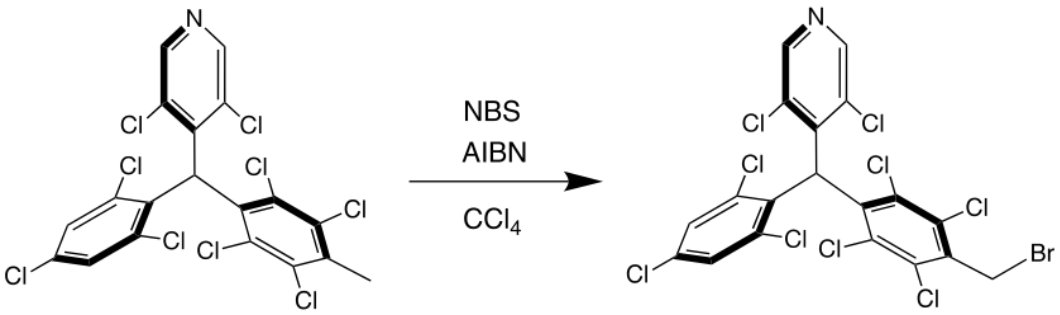

1 **2**

Under a N_2 atmosphere, to a solution of compound **1** (440 mg, 0.77 mmol) in CCl_4 (15 mL) was added a mixture of *N*-bromosuccinimide (NBS) (686 mg, 3.9 mmol) and azobis(isobutyronitrile) (AIBN) (32 mg, 0.19 mmol). The mixture was refluxed for 2 days. During the reaction, NBS (1969 mg, 11 mmol) and AIBN (106 mg, 0.65 mmol) were split into four portions and each portion was added every 6-12 hours. The resulting mixture was cooled, added CCl_4 (15 mL) and filtered. The filtrate was purified by silica gel column chromatography (eluent: CH_2Cl_2) to give colorless oil. Evaporation in vacuo gave white solid of (3,5-dichloro-4-pyridyl)(4-bromomethyl-2,3,5,6-tetrachlorophenyl)(2,4,6-trichlorophenyl)methane (361 mg, 72 %). This crude was used in the next step without further purification. **^{1}H NMR ($CDCl_3$, 500 MHz)**: 4.85 (s, 2H), 6.84 (s, 1H), 7.33 (m, 1H), 7.42 (m, 1H), 8.40 (d, 1H, *J*=8.8 Hz), 8.52 (d, 1H, *J*=10 Hz) **MALDI-TOF-MS**: *m/z* = 648 ($[C_{19}H_7BrCl_9N]^+$).

Synthesis of diethyl (3,5-dichloro-4-pyridyl) (2,4,6-trichlorophenyl)methyl-2,3,5,6-tetrachloro-benzyl phosphonate (3)

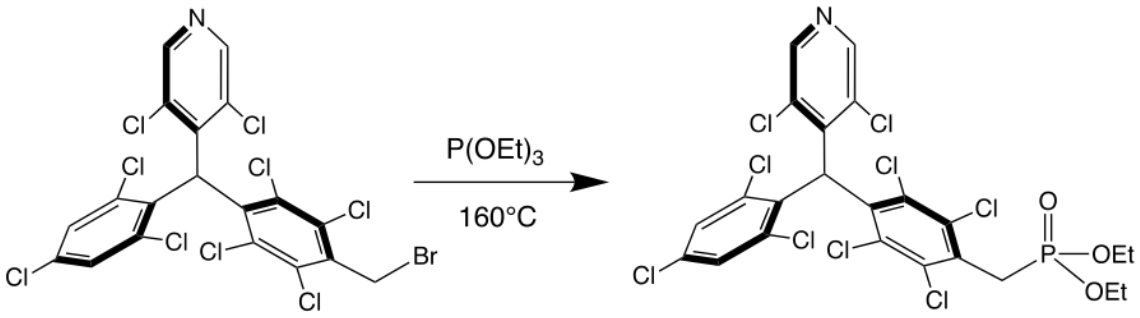

2 **3**

Under an N_2 atmosphere, a solution of compound **2** (196 mg, 0.30 mmol) in $P(OEt)_3$ (0.50 mL, 3.0 mmol) was heated under reflux for 2 h at 160°C. After cooling the resulting solution to room temperature, $P(OEt)_3$ was removed by evaporation. The resulting residue was purified by silica gel column chromatography (eluent: CH_2Cl_2) to yield red oil of compound **3** (111 mg, 52 %). **^{1}H NMR** ($CDCl_3$, 500 MHz): 1.26 (t, 6H, *J*=7.0 Hz), 3.77 (d, 2H, *J*=22.7 Hz), 4.07 (m, 4H), 6.80 (s, 1H), 7.26 (m, 1H), 7.38 (m, 1H), 8.36 (d, 1H, *J*=9.5 Hz), 8.48 (d, 1H, *J*=9.2 Hz). **HRMS (FAB+)**: *m/z* Calcd for $C_{23}H_{17}Cl_9NO_3P$: 701.8221, Found: 701.8226.

Synthesis of αH-TPA-R (4)

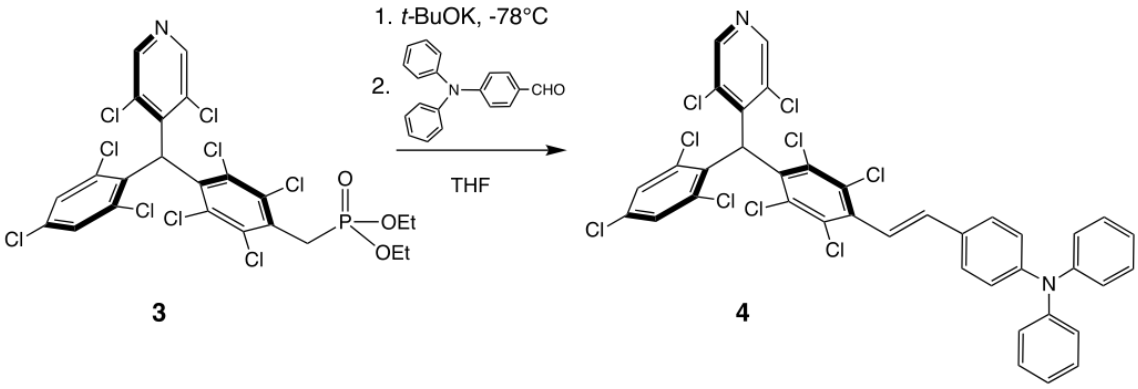

Under a N_2 atmosphere, to a phosphonate compound **3** (63.3 mg, 0.090 mmol), 1 M ^{t}BuOK solution in THF (0.20 mL, 0.197 mmol) was added to a solution of the phosphonate in dry THF (10 mL) at –78°C. The resulting orange solution was stirred for 20 min and was added 4-diphenylaminobenzaldehyde (29.4 mg, 0.108 mmol). The resulting purple solution was warmed up to room temperature and stirred for 18 h. The reaction mixture was extracted with CH_2Cl_2, washed with water and dried ($MgSO_4$). The crude product obtained by evaporation was purified by silica gel column chromatography (eluent: CH_2Cl_2/hexane = 1/1) to yield yellow oil (32.8 mg, 44 %). **^{1}H NMR ($CDCl_3$, 500 MHz)**: 6.36 (d, 1H), 6.74 (d, 1H), 6.84 (s, 1H), 7.04-7.07 (m, 8H), 7.13 (m, 2H), 7.24 (m, 2H), 7.28 (m, 2H), 7.40 (d, 2H), 8.38 (d, 1H), 8.50 (d, 1H). **HRMS (FAB+)**: *m/z* Calcd for $C_{38}H_{22}Cl_9N_2$: 819.8902, Found: 819.8916.

Synthesis of TPA-R•

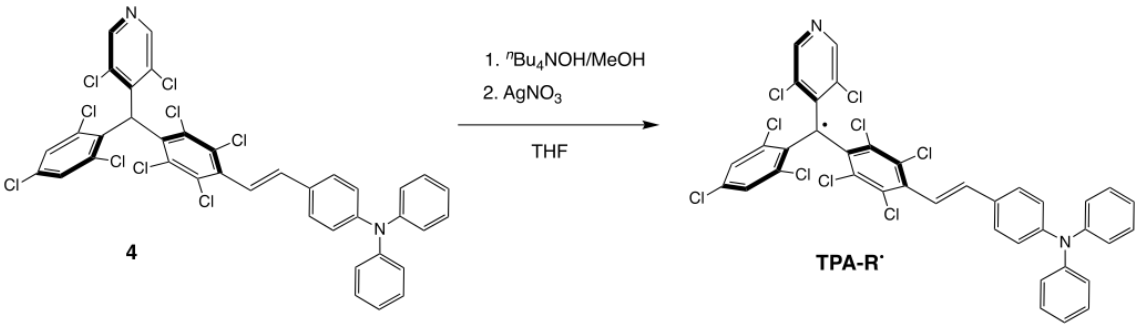

Under a N_2 atmosphere, compound **4** (24 mg, 0.029 mmol) was dissolved in dry THF (24 mL). 1 M $^{n}Bu_4NOH$ solution in THF (0.070 mL, 0.070 mmol) was added. The resulting purple solution was stirred overnight in the dark. Silver(I) nitrate (44 mg, 0.174 mmol) was added and stirred for 3 h. The resulting suspension was filtered, evaporated, purified by Al_2O_3 column chromatography (CH_2Cl_2/hexane = 1/1) and dried in vacuo to afford red oil. Slow evaporation of acetone/ethanol solution provided reddish brown powder (13.9 mg, 58 %). **HRMS (ESI-TOF+)** *m/z* Calcd for $C_{38}H_{21}Cl_9N_2$: 818.8823, Found: 818.8817. HPLC chromatogram (SunFire Silica Prep Column, 100 Å, 5 µm, 4.6 mm × 250 mm, eluent: CH_2Cl_2) showed a single peak attributed to TPA-R•, confirming the high purity.

ESR spectroscopy

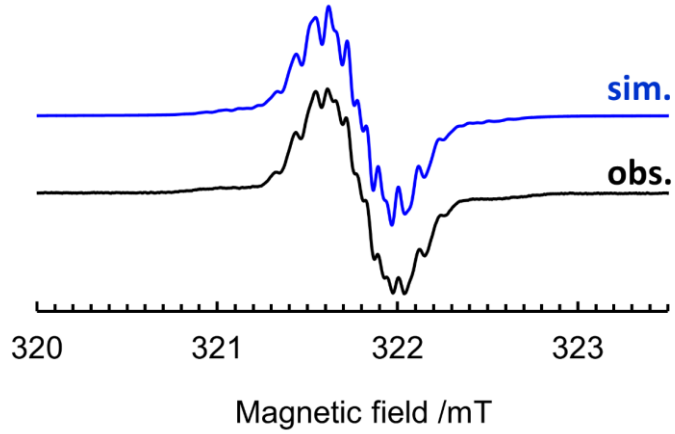

Figure S1 ESR spectrum of the CH_2Cl_2 solution of TPA-R˙ at 175 K (black) and computer simulation (blue). Hyperfine coupling constants used for the simulation are shown in Table S1.

Table S1 Hyperfine coupling constants (mT) used for simulating ESR spectrum and DFT-calculated values.

	N	H_{aryl}	H_{vinyl1}	H_{vinyl2}	ortho-^{13}C	α-^{13}C
Sim.	0.107	0.112[a]	0.163	0.066	1	-
Calcd.	0.1222	0.1338	0.1751	-0.0889	1.0633	3.6508
		0.1335			1.0996	
		0.1516			1.0992	
		0.1423			1.0516	
					1.1035	
					1.1463	

TDDFT calculation for TPA-R•

Table S2 Absorption wavelengths and energies of TPA-R• in cyclohexane and the corresponding transition energies and oscillator strengths calculated by the TD-DFT method using uB3LYP or uCAM-B3LYP functionals with 6-31+G* basis set.

	λ_{max} [a]/nm	E_{max} [a]/eV	E_{calc} [b]/eV	Oscillator Strength[c]	Configuration	Coefficient[d]
uB3LYP	714	1.73	1.30	0.1094	207B→208B	0.991
	482	2.57	2.39	0.0960	206B→208B 208A→209A	0.688 −0.414
	393	3.16	2.71 2.84 2.96 3.20	0.0314 0.7703 0.0790 0.0267	200B→208B 208A→209A 207B→209B 197B→208B 208A→210A	0.819 0.590 0.664 −0.618 0.657
uCAM-B3LYP	714	1.73	–	–	–	–
	482	2.57	2.75	0.1314	206B→208B 207B→208B	0.402 0.411
	393	3.16	3.03	0.3044	207B→208B	0.664

a Absorption maxima
b Corresponding transition energy calculated by TD-DFT method
c Oscillator strength calculated by TD-DFT method
d Major contribution (>0.4) are shown.

Stokes shifts of TPA-R•

Table S3 Absorption and emission spectral data for TPA-R• in cyclohexane and chloroform solution.

	λ_{abs} (nm)	λ_{exc} (nm)	λ_{em} (nm)	Stokes Shift (cm^{-1})
Cyclohexane	714	400	915	3077
Chloroform	733	400	1003	3673

UV-vis-NIR absorption spectroscopy (one-electron oxidation of TPA-R•)

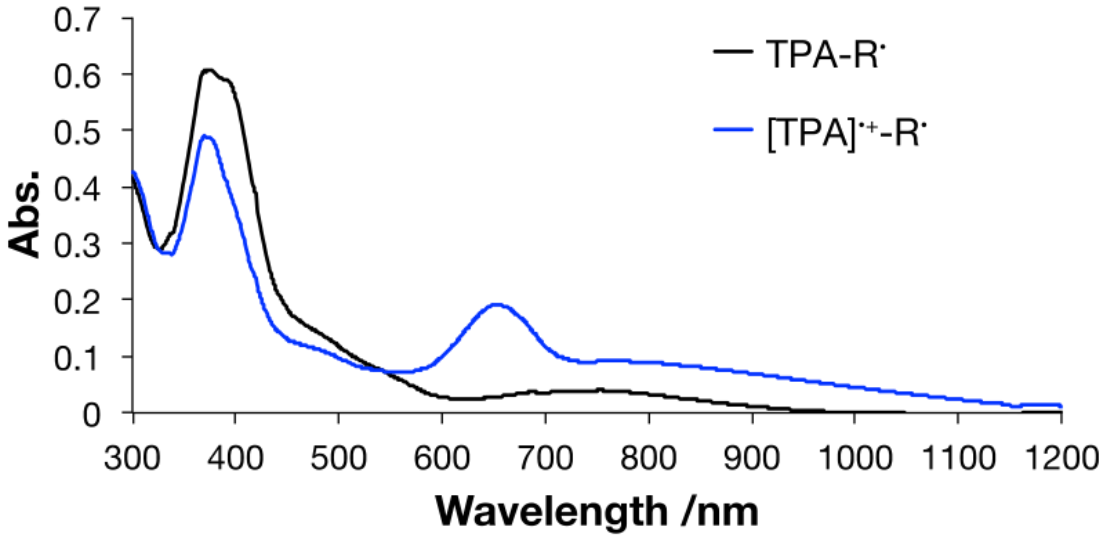

Figure S2 UV-vis-NIR absorption spectra of TPA-R• and $[TPA]^{\bullet+}$-R• in CH_2Cl_2 containing $^{n}Bu_4PF_6$ (0.1 M). $[TPA]^{\bullet+}$-R• was generated in-situ by electrochemical oxidation.

DFT calculation for [TPA-R•][B(C_6F_5)$_3$]

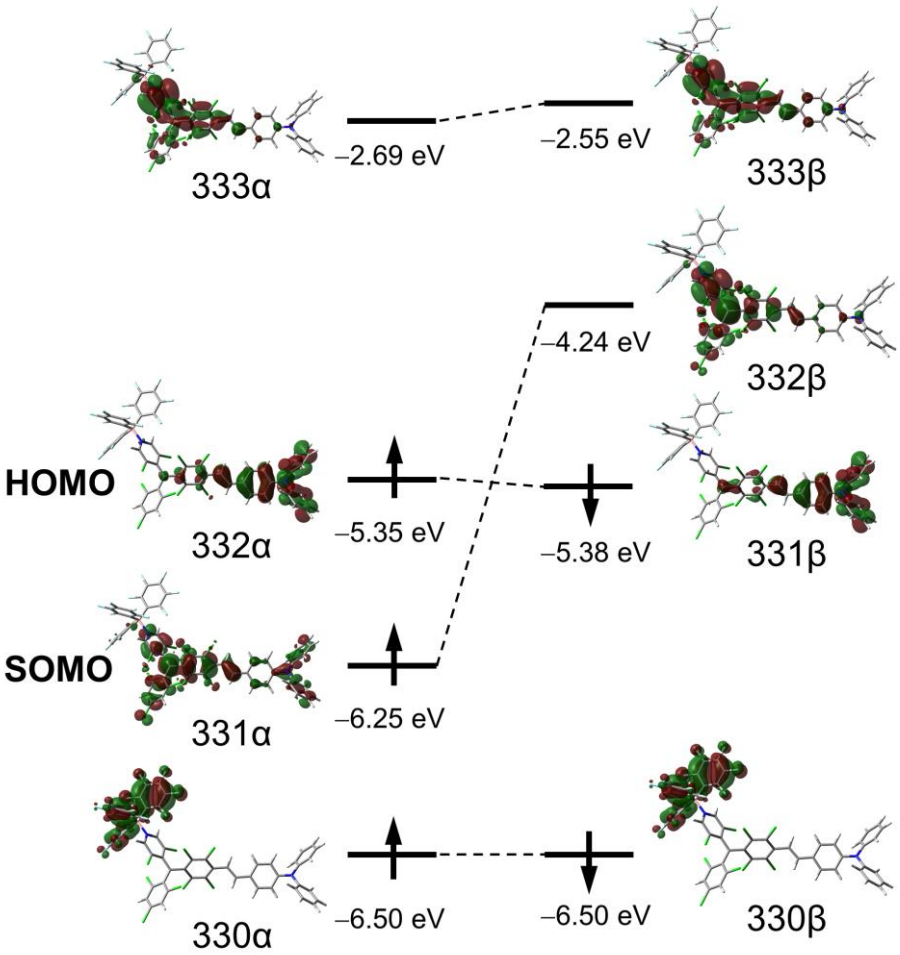

Figure S3 MO diagram for [TPA-R•][B(C_6F_5)$_3$] calculated using DFT (uB3LYP/6-31G*).

UV-vis-NIR absorption spectroscopy (Lewis-acid addition)

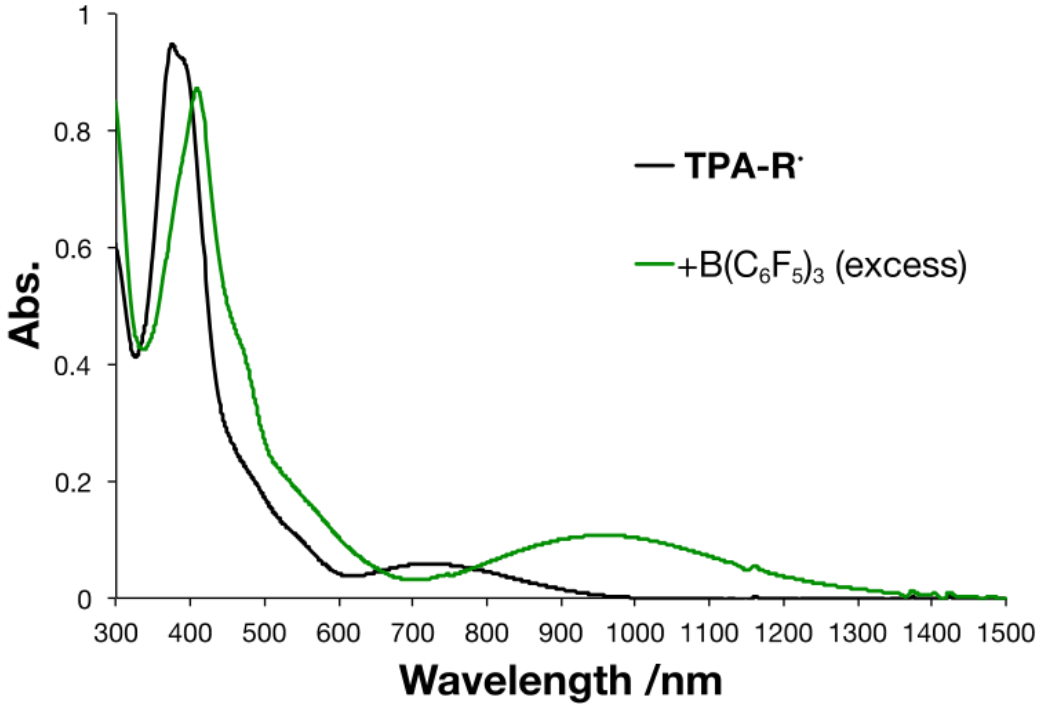

Figure S4 Change in UV-vis-NIR absorption spectra upon addition of $B(C_6F_5)_3$ (Lewis acid) to a CH_2Cl_2 solution of TPA-R•.

Emission spectroscopy (Brønsted-acid addition)

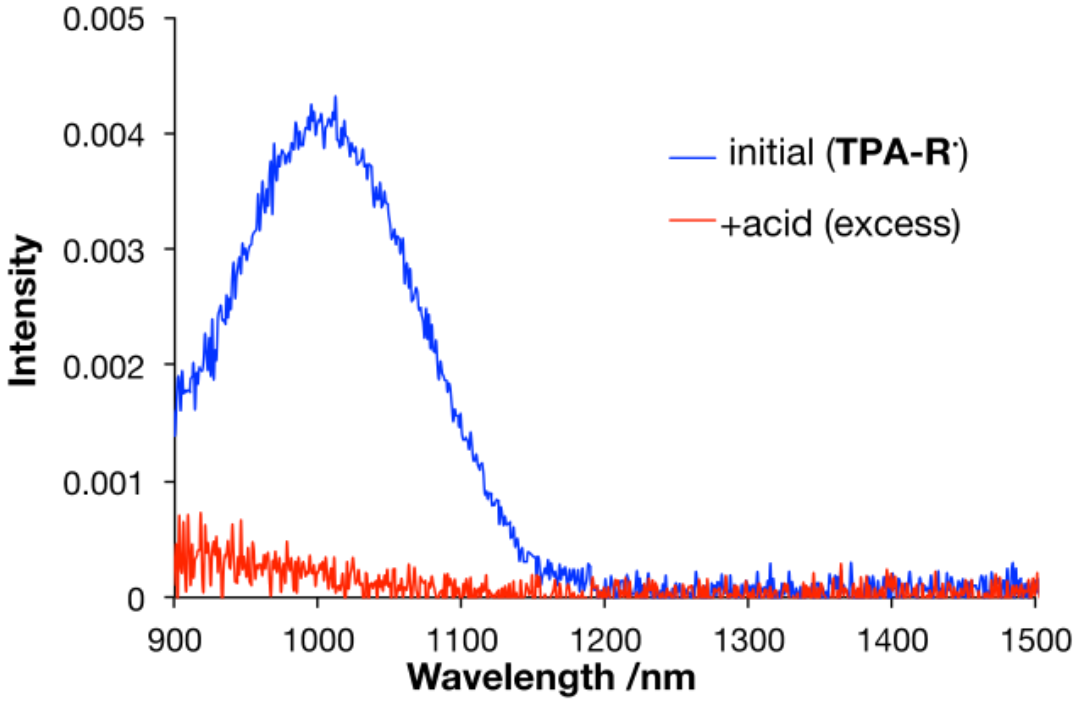

Figure S5 Changes in emission spectra upon addition of CF_3SO_3H (acid) to a cyclohexane/$CHCl_3$ (1/1) solution of TPA-R•.

UV-vis-NIR absorption spectroscopy (Brønsted-acid and base addition)

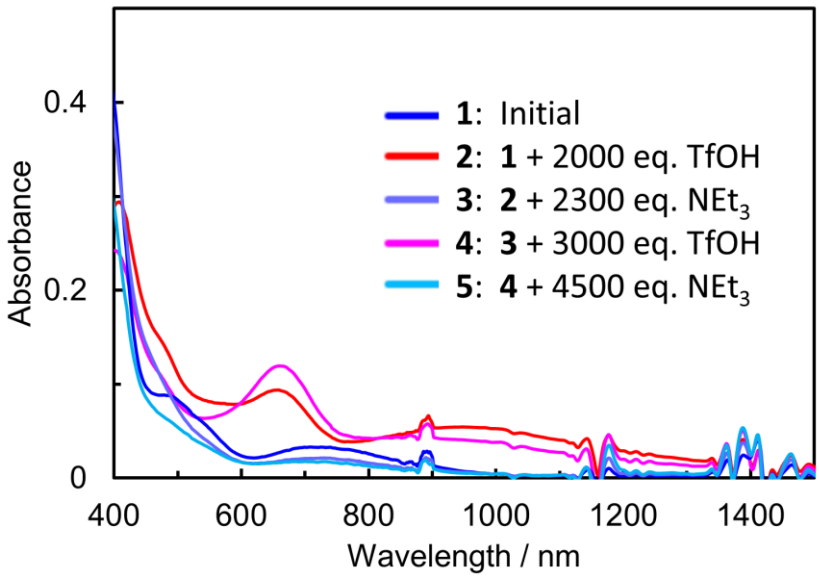

Figure S6 Changes in UV-vis-NIR absorption spectra upon addition of TfOH (acid) and NEt_3 (base) to a CH_2Cl_2 solution of TPA-R$^{\bullet}$.

In Figure S6, the absorbance of the transition band around 650 nm, which is the indicative of the intramolecular electron transfer, is larger in **4** than in **2**. This would probably be due to the enhanced polarity of the solution by larger amount of the salt $(NEt_3H)OTf$ in **4**. The enhanced polarity is expected to facilitate the intramolecular electron transfer.

Excitation spectrum of TPA-R•

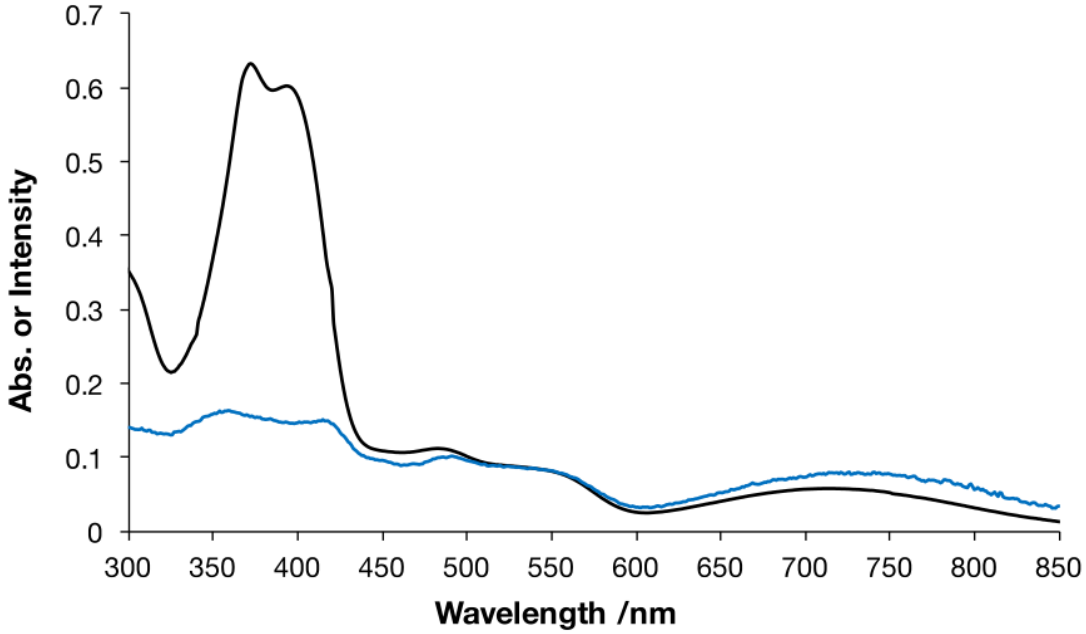

Figure S7 Excitation spectrum of TPA-R• observed for emission wavelength at 907 nm (blue line) and absorption spectrum of TPA-R• (black line) in a cyclohexane solution.

Schematic descriptions of photoexcitation and carrier injection

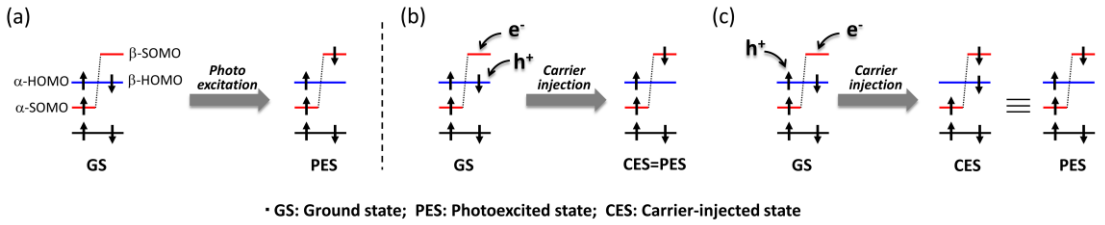

Figure S8 Schematic (a) photoexcitation (b, c) and two possible carrier injection processes of radicals with a SOMO-HOMO converted non-Aufbau electronic structure. Blue and red lines indicate the energy levels of the HOMO (electron-donor centered orbital) and SOMO (radical-centered orbital). For simplicity, the energy levels of α- and β-orbitals other than SOMOs are assumed to degenerate.

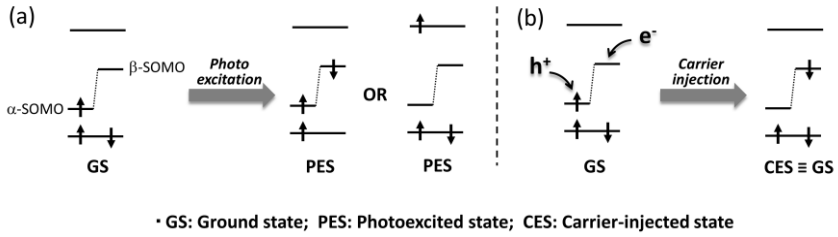

Figure S9 Schematic (a) photoexcitation (b) and carrier injection processes of radicals with conventional Aufbau orbital configuration. For simplicity, the energy levels of α- and β-orbitals other than SOMOs are assumed to degenerate.

As shown in Figure S8a, photoexcitation of a radical with a SOMO-HOMO converted non-Aufbau electronic structure transfers an electron from the β-HOMO to the β-SOMO, then the radical in the photoexcited state (PES) has two electrons in its radical-centered orbital (shown in red) and one electron on its electron-donor centered orbital (shown in blue). Upon carrier injection into the radical, the electron is expected to be injected to the β-SOMO, which is an empty orbital with the lowest energy, while hole is assumed to be injected into either α- or β-HOMOs (Figure S8b,c), which are filled orbitals with the highest energy. As shown in Figure S8b and S8c, the carrier injected state (CES) is identical to the PES in these two cases. We note that, in Figure S8c, the CES looks different from the PES, but this difference originates from the way of depicting spin configuration in the CES, in which α- and β-electron should become β- and α-electrons, on the basis of the number of their total electrons (α- and β-electrons are defined in such a way that total number of electron is larger in α than in β) Indeed, we can confirm that both the CES and PES have two electrons in its radical-centered orbital (shown in red)

and one electron on its electron-donor centered orbital (shown in blue), and that the spin multiplicity of CES and PES is the same (= doublet). Consequently, carrier injection can form the PES in this type of radicals.

In case of radicals with conventional Aufbau orbital configuration, α- or β-electron are photoexcited to form the PES upon photoexcitation (Figure S9a), while the hole and electron are injected into α- and β-SOMOs, respectively, to yield the CES upon electrical excitation (Figure S9b). The resulting CES is not the PES but the GS. According to this simple consideration, the carrier injection does not produce the PES but afford the GS in this type of radicals.

Cyclic voltammograms of the related compounds

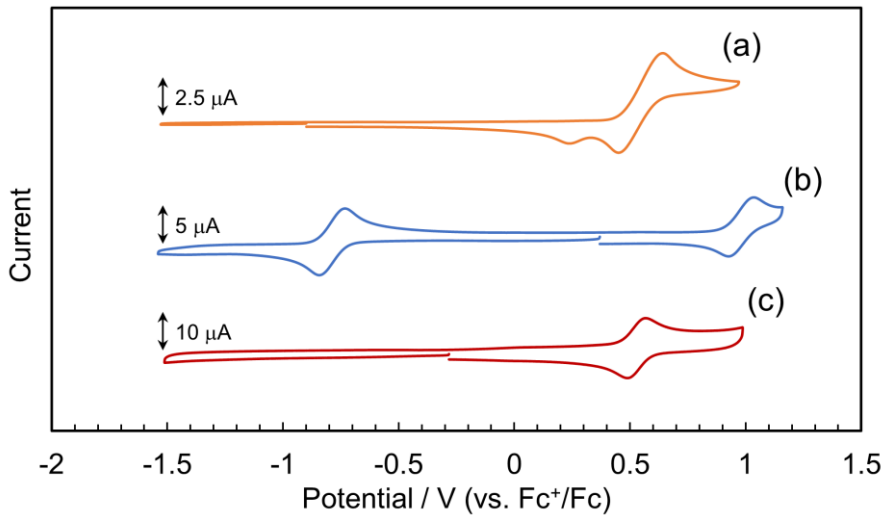

Figure S10 Cyclic voltammograms of (a) TPA, (b) PyBTM, and (c) **4** in CH_2Cl_2 containing 0.1 M $^nBu_4NPF_6$, obtained at a scan rate of 0.1 V s^{-1}.

The reduction potential of TPA-R$^\bullet$ ($E^{0\prime}_1 = -0.69$ V vs. Fc^+/Fc) is close to that of PyBTM ($E^{0\prime}_1 = -0.79$ V) while **4** does not show any reduction waves in this potential region. These results indicate that the first reduction of TPA-R$^\bullet$ is attributed to the diphenylpyridylmethyl radical moiety. On the other hand, the oxidation potential of TPA-R$^\bullet$ ($E^{0\prime}_2 = 0.38$ V) is close to that of **4** ($E^{0\prime}_1 = 0.53$ V) while less positive than that of PyBTM ($E^{0\prime}_2 = 0.98$ V), suggesting that the first oxidation TPA-R$^\bullet$ occurs mainly at the TPA moiety. These results support the SOMO–HOMO converted electronic structure of TPA-R$^\bullet$.

Photoemission yield spectroscopy

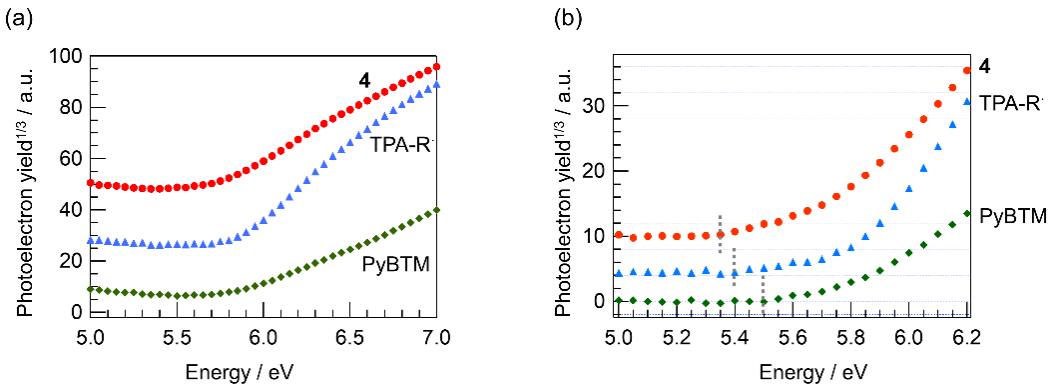

Figure S11 Photoemission yield spectra of related compounds. (a) Raw data and (b) baseline-corrected data. The spectra of **4** (red) and TPA-R$^{\bullet}$ (blue) were shifted to upper direction for clarity. Gray dotted lines in (b) indicate estimated ionization potentials. The compounds were spin-coated or drop-casted on ITO substrates.

Photostability examination

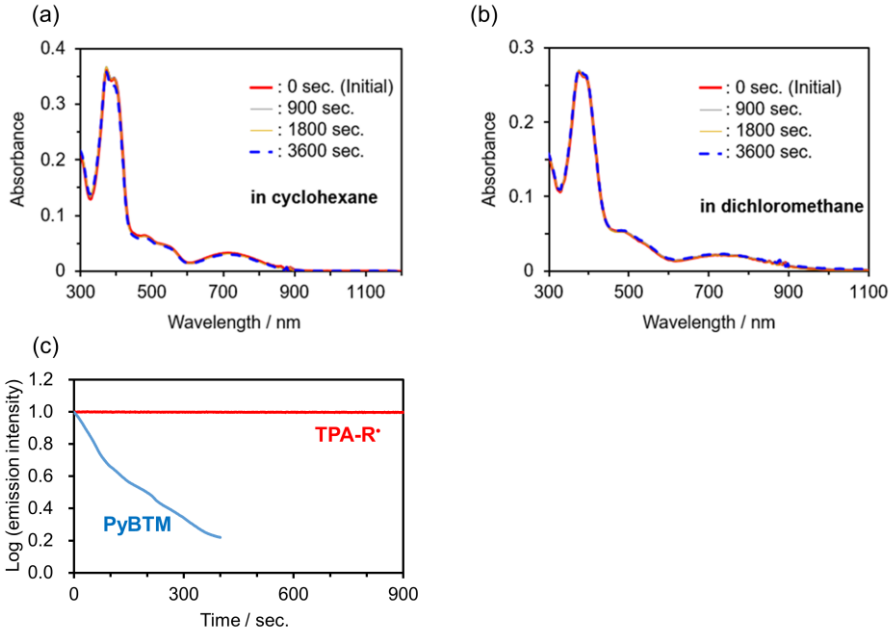

Figure S12 Time-dependent absorption spectra of TPA-R• in cyclohexane (a) and in dichloromethane (b) upon continuous photoirradiation at λ_{ex} = 400 nm. (c) Time-dependent emission intensities of TPA-R• and PyBTM in cyclohexane upon continuous photoirradiation at λ_{ex} = 400 and 370 nm, respectively.

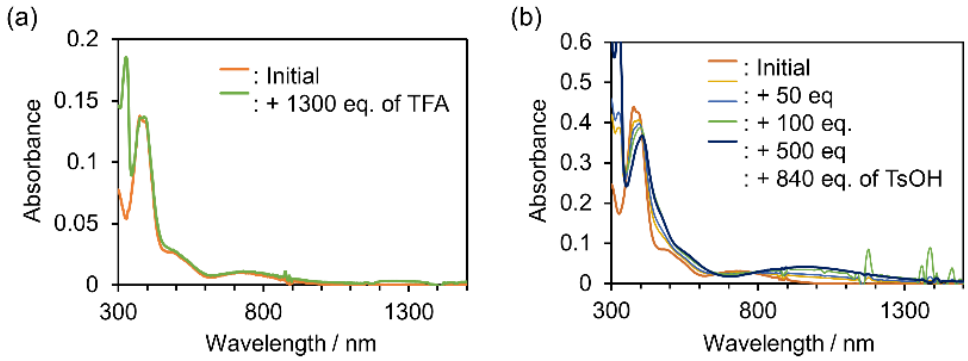

Figure S13 UV–vis–NIR absorption spectra upon the addition of (a) trifluoroacetic acid or (b) tosylic acid to TPA-R$^{\bullet}$ in CH_2Cl_2/CH_3CN (5/1). Intramolecular electron transfer was not observed in both cases.

MO diagrams calculated using uCAM-B3LYP functional

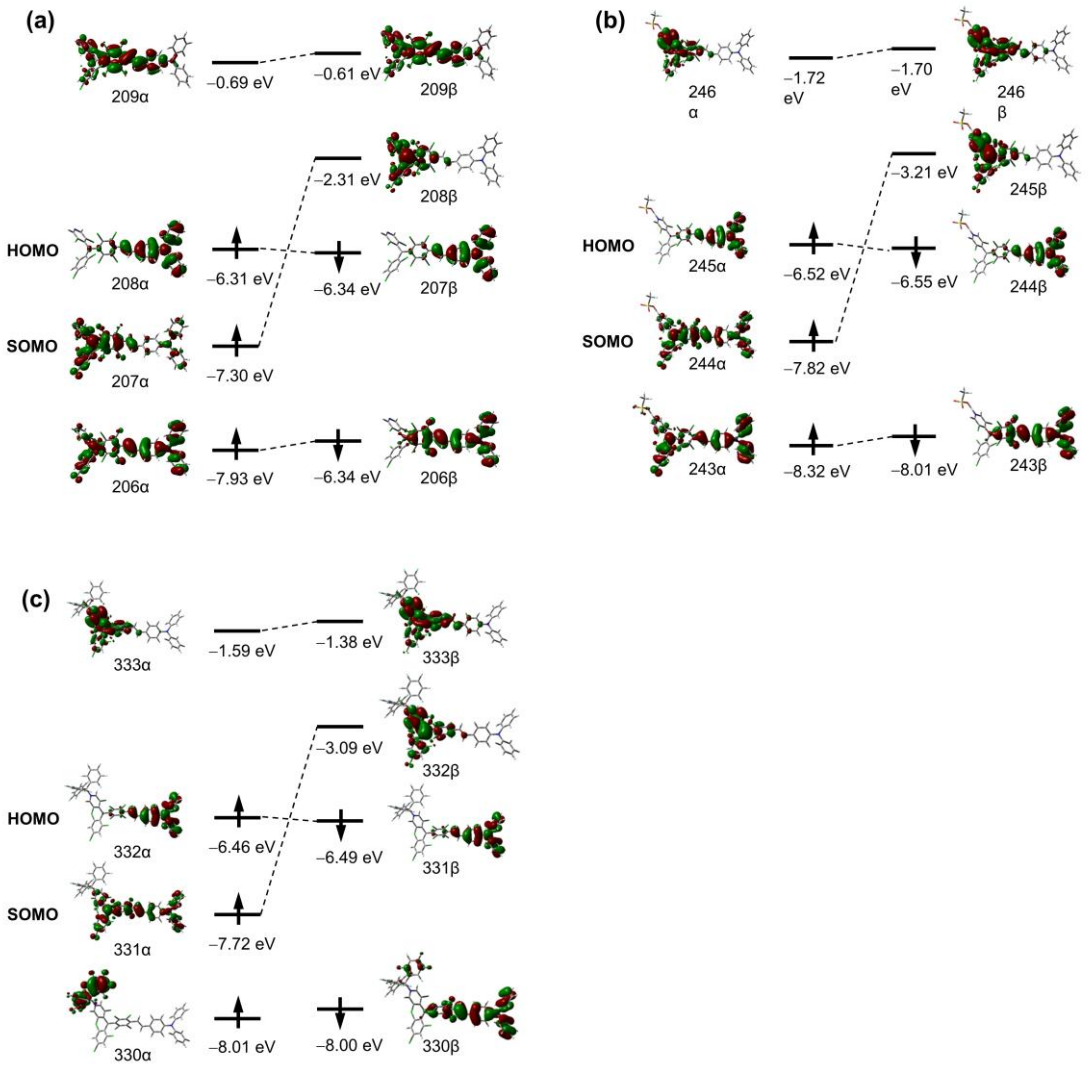

Figure S14 MO diagrams for (a) TPA-R$^{\bullet}$, (b) [TPA-RH$^{\bullet}$]OTf, and (c) [TPA-R$^{\bullet}$][B(C_6F_5)$_3$] calculated using DFT (uCAM-B3LYP/6-31G*).

UV-vis-NIR absorption spectroscopy upon gradual addition of TfOH

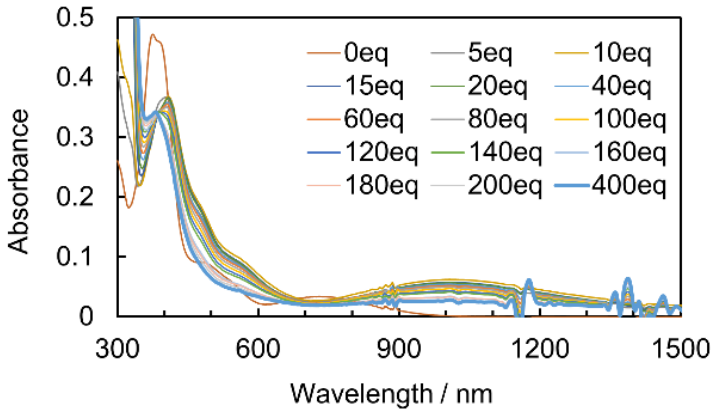

Figure S15 UV-vis-NIR absorption spectra upon gradual addition of TfOH to TPA-R$^{\bullet}$ in CH_2Cl_2/CH_3CN (5/1). The electronic transition band around 650 nm attributed to an intramolecular electron transfer was not detected even under addition of 400 eq. of TfOH.

Cyclic voltammetry upon titration with TfOH

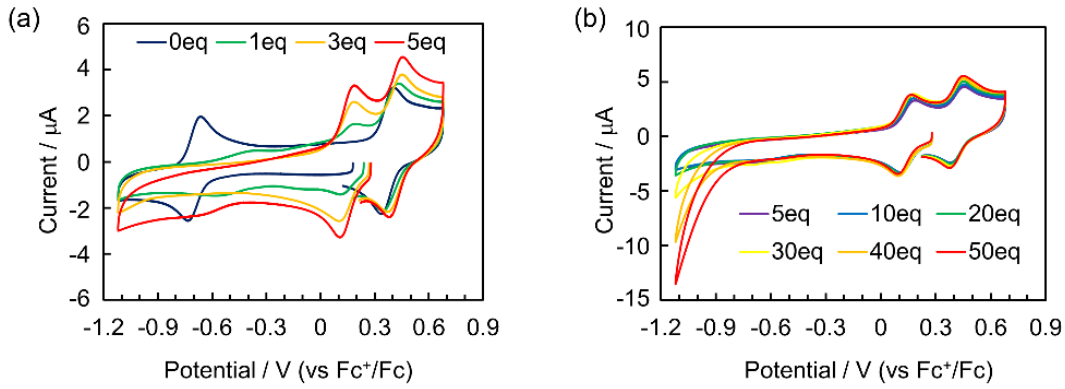

Figure S16 Cyclic voltammograms of TPA-R$^{\bullet}$ in CH_2Cl_2 containing 0.1 M $^{n}Bu_4NPF_6$ obtained at a scan rate of 0.1 $V \cdot s^{-1}$ upon addition of TfOH. (a) 0 to 5 eq. of TfOH. (b) 5 to 50 eq. of TfOH.

Parameters for simulating a IVCT band

Table S4 Parameters for simulating the IVCT band in the absorption spectrum of TPA-R•.

Solvent	r_{DA} / Å[a]	ν_{max} / cm^{-1}	ε_{max} / $M^{-1}cm^{-1}$	$\Delta\nu_{1/2}$ / cm^{-1}	H_{ab} / cm^{-1} [b]
Cyclohexane	12.4	14096	1435	3419	437
Toluene	12.4	13479	1215	3311	387
Chloroform	12.4	13730	1106	3855	402
Dichloromethane	12.4	13355	1369	4406	472
Acetonitrile	12.4	13935	944	4081	385

a: Distance between the nitrogen atom at the triphenylamine moiety and the centering carbon atom at the triarylmethyl radical moiety estimated from DFT-optimized structure.
b: Electronic coupling H_{ab} was estimated by analyzing the lowest-energy transition band in absorption spectra based on the Hush theory ($H_{ab} = 0.0206(\nu_{max}\varepsilon_{max}\Delta\nu_{1/2})^{1/2} / r_{DA}$).[12,13]

Solvent-dependent optical properties

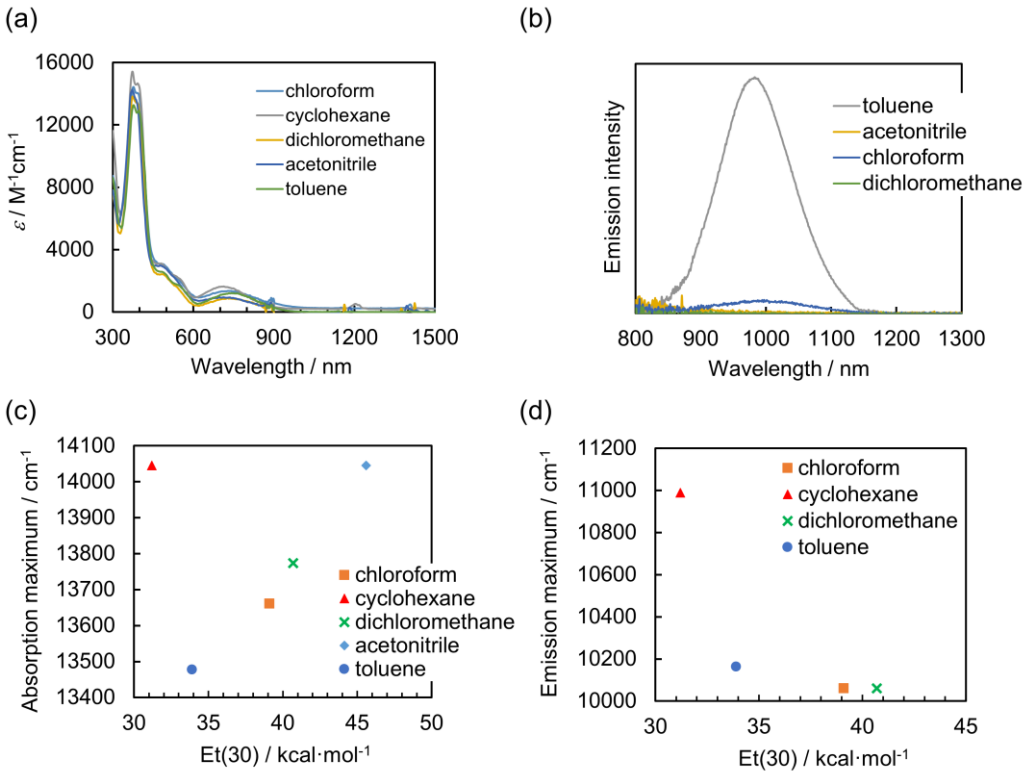

Figure S17 Solvent-dependent (a) absorption and (b) emission spectra of TPA-R$^{\bullet}$ in various solvents with different polarity. The (c) absorption and (d) emission peak maxima were plotted against Et(30).

As the solvent polarity increased, the peak energy of the lowest-energy absorption band increased while that of the emission band decreased, except for cyclohexane. These two trends are presumably resulted from the competition between the increase of the solvent reorganization energy (λ_o) and the decrease of ΔG^{00}.[14] Charge transfer excited state has zwitterionic character and is more polar than the ground state, thus ΔG^{00} decreases and λ_o increases as the solvent polarity increases. Judging from the experimentally obtained solvent dependence, λ_o would affect more than ΔG^{00} in the present case.

Emission decay curve

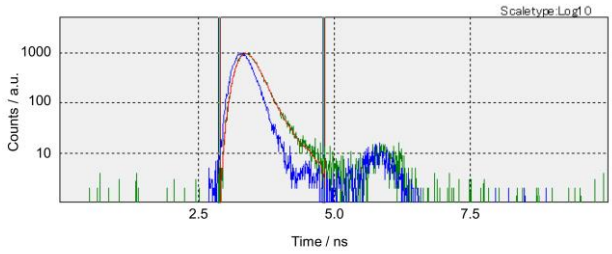

Figure S18 Emission decay curve (green) at λ = 915 nm of TPA-R$^{\bullet}$ upon photoexcitation (λ_{ex} = 405 nm). Blue and red lines indicate instrument response function and fitting curve with τ_1 = 0.08 ns (A_1 = 123) and τ_2 = 0.43 nm (A_2 = 3.93), respectively. τ_{ave} = 0.13 ns is estimated using an equation: $\tau_{ave} = (\tau_1^2 A_1 + \tau_2^2 A_2) / (\tau_1 A_1 + \tau_2 A_2)$.

References

(1) Gaussian 09 revision C01, Frisch, M. J.; Trucks, G. W.; Schlegel, H. B.; Scuseria, G. E.; Robb, M. A.; Cheeseman, J. R.; Scalmani, G.; Barone, V.; Mennucci, B.; Petersson, G. A.; Nakatsuji, H.; Caricato, M.; Li, X.; Hratchian, H. P.; Izmaylov, A. F.; Bloino, J.; Zheng, G.; Sonnenberg, J. L.; Hada, M.; Ehara, M.; Toyota, K.; Fukuda, R.; Hasegawa, J.; Ishida, M.; Nakajima, T.; Honda, Y.; Kitao, O.; Nakai, H.; Vreven, T.; Montgomery, J. A., Jr.; Peralta, J. E.; Ogliaro, F.; Bearpark, M.; Heyd, J. J.; Brothers, E.; Kudin, K. N.; Staroverov, V. N.; Kobayashi, R.; Normand, J.; Raghavachari, K.; Rendell, A.; Burant, J. C.; Iyengar, S. S.; Tomasi, J.; Cossi, M.; Rega, N.; Millam, M. J.; Klene, M.; Knox, J. E.; Cross, J. B.; Bakken, V.; Adamo, C.; Jaramillo, J.; Gomperts, R.; Stratmann, R. E.; Yazyev, O.; Austin, A. J.; Cammi, R.; Pomelli, C.; Ochterski, J. W.; Martin, R. L.; Morokuma, K.; Zakrzewski, V. G.; Voth, G. A.; Salvador, P.; Dannenberg, J. J.; Dapprich, S.; Daniels, A. D.; Farkas, Ö.; Foresman, J. B.; Ortiz, J. V.; Cioslowski, J.; Fox, D. J. Gaussian, Inc., Wallingford CT, 2009.

(2) Becke, A. Density-functional exchange-energy approximation with correct asymptotic behavior. *Phys. Rev. A* **1988**, *38*, 3098–3100.

(3) Becke, A. Density-functional thermochemistry. III. The role of exact exchange. *J. Chem. Phys.* **1993**, *98*, 5648–5652.

(4) Lee, C.; Yang, W.; Parr, R. Development of the Colle-Salvetti correlation-energy formula into a functional of the electron density. *Phys. Rev. B* **1988**, *37*, 785–789.

(5) Yanai, T.; Tew, D.; Handy, N. A new hybrid exchange-correlation functional using the Coulomb-attenuating method (CAM-B3LYP), *Chem. Phys. Lett.*, **2004**, *393*, 51-57.

(6) Hariharan, P.; Pople, J. The influence of polarization functions on molecular orbital hydrogenation energies. *Theoretica Chimica Acta* **1973**, *28*, 213–222.

(7) Rassolov, V.; Ratner, M.; Pople, J.; Redfern, P.; Curtiss, L. 6-31G* basis set for third-row atoms. *J. Comput. Chem.* **2001**, *22*, 976–984.

(8) Lipparini, F.; Scalmani, G.; Mennucci, B.; Cances, E.; Caricato, M.; Frisch, M.J. A variational formulation of the polarizable continuum model, J. Chem. Phys., **2010**, *133*, 014106.

(9) Reindl, S.; Penzkofer, A.; Gong, S.-H.; Landthaler, M.; Szeimies, R. M.; Abels, C.; Baumler, W. Quantum Yield of Triplet Formation for Indocyanine Green. *J. Photochem. Photobiol. A: Chem.* **1997**, *105*, 65–68.

(10) Ishida, H.; Bünzli, J.; Beeby, A. Guidelines for measurement of luminescence spectra and quantum yields of inorganic and organometallic compounds in solution and solid state (IUPAC Technical Report). *Pure Appl. Chem.* **2016**, *88*. 701–711.

(11) Bertini, V.; Lucchesini, F.; Pocci, M.; De Munno, A. 3,5-Dichloro-4-pyridinecarbonitrile as a Key Reagent in a Synthesis of Copper Containing Amine Oxidase Inhibitors. *Heterocycles.* **1995**, *41*, 675–688.

(12) Hush, N. S. *Prog. Inorg. Chem*. Intervalence-Transfer Absorption. Part 2. Theoretical Considerations and Spectroscopic Data. **1967**, *8*, 391−444.

(13) Hush, N. S. Homogeneous and heterogeneous optical and thermal electron transfer. *Electrochim. Acta* **1968**, *13,* 1005−1023.
(14) Heckmann, A.; Lambert, C.; Goebel, M.; and Wortmann R. Synthesis and Photophysics of a Neutral Organic Mixed-Valence Compound. *Angew. Chem. Int. Ed.* **2004**, *43*, 5851–5856.